論文 / 著書情報
Article / Book Information

Title	Perpendicular Magnetic Anisotropy in Full-Heusler Co2FeSi Alloy and MgO Bilayers
Authors	Y. Takamura, Y. Stutler, E. Matsushita, K. Shinohara, T. Suzuki, S. Nakagawa
Citation	J. Magn. Soc. Jpn., Vol. 43, No. 6, pp. 120-124
Pub. date	2019, 11
Copyright	本著作物の著作権は 公益社団法人日本磁気学会 (The Magnetics Society of Japan)が保有しています。
Note	This file is author (final) version.

Perpendicular magnetic anisotropy in full-Heusler Co_2FeSi alloy and MgO bilayers

Y. Takamura, Y. Stutler, E. Matsushita, K. Shinohara, T. Suzuki, and S. Nakagawa

Dept. of Electrical and Electronic Engineering, School of Eng., Tokyo Institute of Technology, *2-12-1 Ookayama, Meguro-ku, Tokyo 152-8552, Japan*

We systematically investigated perpendicular magnetic anisotropy (PMA) in bilayers comprising ultrathin full-Heusler Co_2FeSi (CFS) alloy and MgO as an insulator. The MgO layer was fabricated using two different sputtering techniques: reactive sputtering and radio-frequency sputtering. The characteristics of the layers fabricated using the different methods were compared. Irrespective of the MgO fabrication technique, the CFS/MgO bilayers exhibited PMA when the CFS surface was exposed to oxygen, which resulted in additional Fe–O bonds at the interface. Additionally, we characterized PMA in the bilayers while varying the substrate temperature T_S for CFS sputtering. CFS samples that were 0.6-nm thick exhibited PMA when they were formed at T_S as high as 300°C. The bilayer formed at 350°C exhibited in-plane magnetic anisotropy. Quantitative analysis of the magnetic anisotropy energy density revealed that the dominant magnetic anisotropy contribution in PMA differed between the bilayers formed at 300°C and 350°C. We expect these findings to be useful in the further development of high spin-polarized ferromagnetic electrodes containing PMA for next-generation spintronics devices.

Key words: Half-metallic ferromagnet, HMF, perpendicular magnetic anisotropy, PMA, full-Heusler alloys, MgO-induced magnetic anisotropy

1. Introduction

Half-metallic ferromagnet (HMF)[1)2)] thin films containing perpendicular magnetic anisotropy (PMA)[3)] are attractive as ferromagnetic materials for next-generation magnetoresistive random access memory[4)] and racetrack memory.[5)] The extremely high spin polarization in a HMF leads to highly spin-polarized electrons in such magnetoresistive devices, efficiently yielding a very large tunnel magnetoresistance (TMR) or a high spin-transfer torque (STT).[6)]

Magnetostrictive devices based on PMA exhibit features superior to those containing in-plane magnetic anisotropy (IMA) including high scalability and low energy consumption for magnetization switching.[7)] The critical current density J_{C0} for the STT-effect current-induced magnetization switching can be dramatically decreased as the thermal stability of a ferromagnetic film remains constant.

Numerous Co-based full-Heusler alloys such as Co_2FeSi (CFS),[8)–10)] Co_2MnSi (CMS),[11)12)] and $Co_2Mn_{0.5}Fe_{0.5}Si$[13)] are theoretically expected to be HMFs. Half-metallicity has been experimentally demonstrated in some of these alloys.[13)14)] However, because of the highly symmetric crystal structure, full-Heusler alloys show little crystal anisotropy. Thus, a thin film of a full-Heusler alloy has the easy axis in the plane.

Two approaches are known to induce PMA in such ferromagnetic thin films. One approach involves forming a superlattice with ultrathin layers, such as $[Co/Pt]_n$ superlattices, to yield interfacial anisotropy.[15)] We have previously reported that superlattices of ultrathin CMS and Pd layers exhibit PMA.[11)] We determined that the PMA was strongly dependent on the surface configuration and thus occurred only when the superlattices formed on the MgO(111) substrate. Although the PMA energy density was as high as values typically reported for a conventional CoFeB/MgO system,[16)] this technique is not compatible with MgO(001)-tunnel barrier technology to attain high TMR.[17)] Recently, superlattices comprising two different non-half-metallic full-Heusler alloys with (001) orientation were reported to exhibit half-metallicity with PMA.[18)]

Another approach is to form bilayers with MgO to induce interfacial PMA, similar to the effect observed in the CoFeB/MgO system.[16)] The origin of this PMA is considered to be hybridization[19)] of the Fe 3d and O 2p orbitals; this technique is therefore widely used with Fe-containing alloys, including full-Heusler alloys. Wen et al. first reported PMA in an ultrathin full-Heusler alloy/MgO bilayer with Co_2FeAl.[20)] We have also achieved MgO-interface-induced PMA for CFS,[9)10)] which is theoretically a half-metal.[21)] Many other groups have also studied MgO-induced PMA for various types of Co-based full-Heusler alloys.[22)23)]

We have thus far demonstrated PMA in CFS/MgO bilayers in which the MgO layers were formed via two different techniques: reactive sputtering from Mg metallic targets with an $Ar–O_2$ gas mixture[9)] and radio-frequency (RF) sputtering from MgO insulating targets with pure Ar gas.[10)] In the present paper, we compare these two fabrication techniques and discuss their influence on PMA. In addition, we characterized the substrate temperature dependence of the PMA for the samples with RF-sputtered MgO layers and found that the mechanism of the anisotropy differs for the samples formed at a substrate temperature T_S greater than 300°C.

2. Experimental

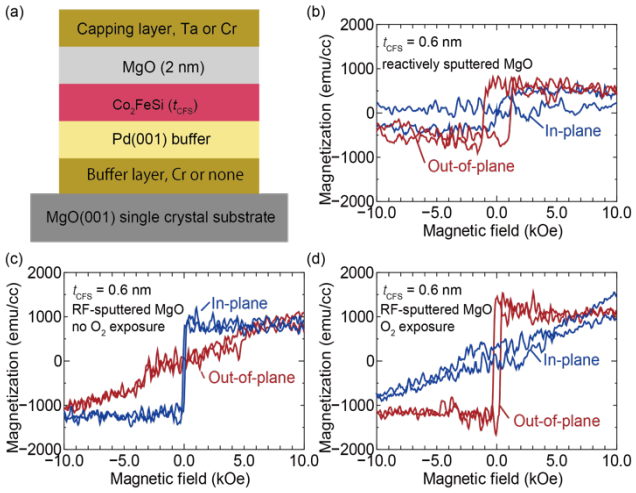

Fig. 1 (a) Schematic of a full stack of samples with a CFS/MgO bilayer. (b–d) *M*–*H* curves for CFS/MgO bilayers. The MgO layer was formed by (b) reactive sputtering and (c,d) RF sputtering. (d) The CFS surface was exposed to oxygen prior to RF sputtering of MgO layers.[9,10]

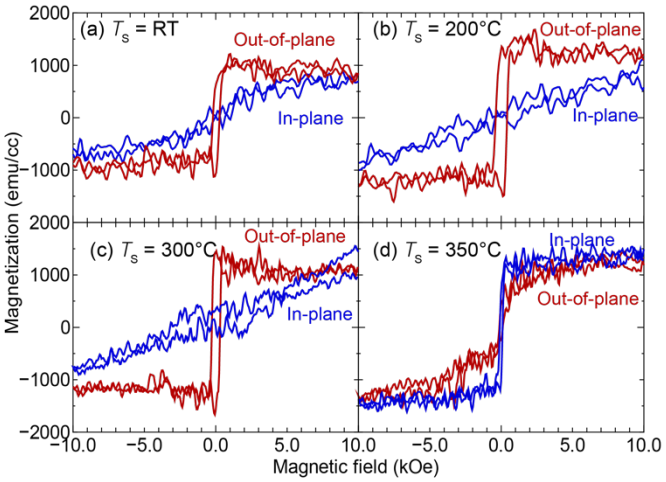

Fig. 2 *M*–*H* loops for CFS (0.6 nm)/MgO bilayers formed at (a) T_S = RT, (b) T_S = 200°C, (c) T_S = 300°C, and (d) T_S = 350°C. The MgO layers were RF sputtered and the surface of CFS was exposed to an oxygen atmosphere.

2.1 Fabrication method

We used a facing target sputtering system equipped with multi sputtering sources and a load-lock chamber to fabricate all of the samples. The base pressure of the sputtering chamber was 10^{-4} Pa. All of the samples were prepared on MgO single crystal substrates with (001) orientation.

A stack of samples is illustrated in Fig. 1(a). Ultrathin CFS and MgO bilayers were formed on (001)-oriented Pd layers. CFS layers were deposited from stoichiometric targets with dc plasma with pure Ar gas. MgO layers were formed either via reactive sputtering from Mg metallic targets at 0.13 Pa in Ar and an O_2 gas mixture with approximately O_2 1% or via RF sputtering from MgO targets at 0.13 Pa in pure Ar. The T_S during CFS was 300°C unless otherwise noted. The MgO layers were formed at room temperature (RT) and capped with either Ta or Cr layers to prevent degradation in the environment.

2.2 Characterization method

Crystallographic properties were characterized by X-ray diffraction. The chemical composition was measured by inductivity coupled plasma optical emission spectrometry (ICP-OES). Magnetic properties were characterized with a vibrating sample magnetometer.

3. Results and Discussion

3.1 Basic characterization of CFS layers

The chemical composition of the sputtered CFS layers was 52 at.% Co, 25 at.% Fe, and 23 at.% Si, which were slightly off-stoichiometric because the sputtering efficiency varies by element. The thick (~30 nm) CFS layers formed at T_S = RT and 200°C on the Pd(001) buffer layers had the *B*2 structure, as indicated by the appearance of (200) diffraction peaks with no (111) diffraction. When the CFS layers were formed at temperatures above T_S = 300°C, (111) diffraction peaks were observed; these layers thus had the $L2_1$ structure.[8] The saturation magnetization of a 100-nm-thick CFS film on the Pd buffer was 1100 emu/cm^3, which is very similar to the bulk value.[24]

3.2 Comparison between MgO formed by reactive sputtering and that formed by RF sputtering

Figure 1(b) and 1(c) compares *M*–*H* loops for the CFS/MgO bilayers in which the MgO layers were formed via reactive and RF sputtering, respectively. The CFS thickness was 0.6 nm. The sample whose MgO layer was reactively sputtered clearly exhibited PMA, whereas the sample with an RF-sputtered MgO layer exhibited IMA. The absence of PMA in the RF-sputtered samples is attributable to an interfacial structure with few Fe–O bonds, which resulted in much weaker interfacial anisotropy than shape magnetic anisotropy.

By comparing the fabrication procedures after the step-by-step deposition of the CFS layers, we observed that oxygen gas with a relatively high partial pressure was introduced to strike plasma for RF-sputtering Mg targets in the oxide mode prior to the sputtering. Then, to form the interface using similar procedures, we exposed the surface of the CFS layer to pure O_2 at 2 Pa for 10 min, equivalent to 9ML (mega Langmuir), before RF-sputtering. The sample prepared in conjunction with the oxygen treatment demonstrated very clear PMA, as shown in Fig. 1(d). The sample with 0.9 ML also exhibited PMA.

We also fabricated a sample with no MgO layer but with the surface exposed to oxygen as a control sample; it exhibited no PMA. This result indicates that PMA originates from the interfaces rather than from the CFS layer, which might be oxidized. The saturation magnetization M_S did not change with the oxygen

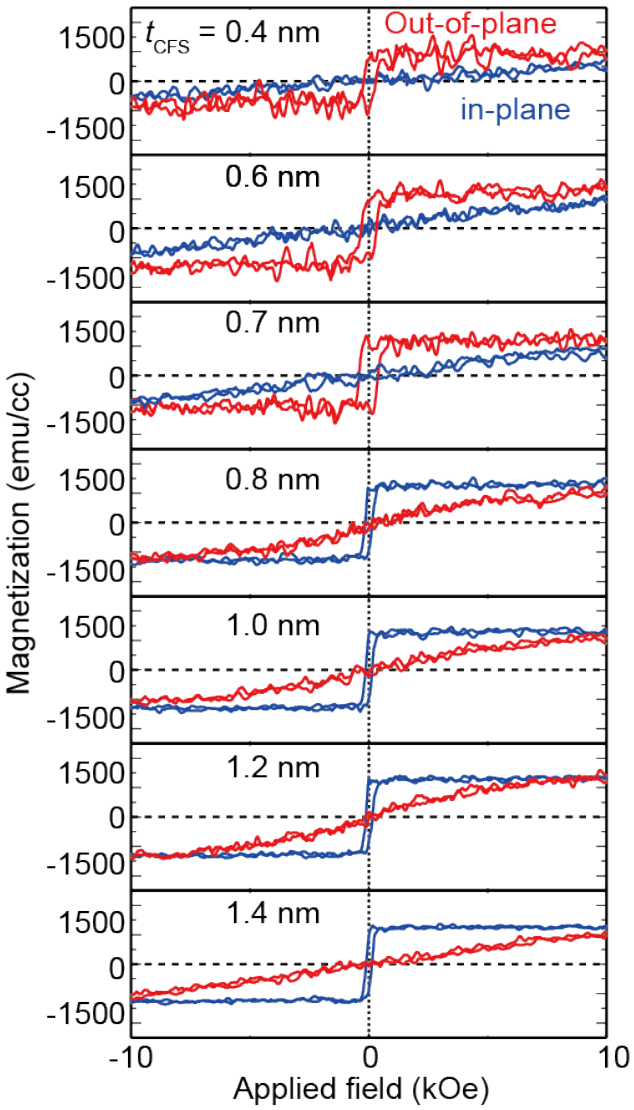

Fig. 3 Magnetization vs field curves for CFS/MgO bilayers formed at T_S = 300°C. The thickness of the CFS layers was varied from 0.4 nm to 1.4 nm.

exposure; thus, this result further suggests that the CFS was not oxidized. Only the surface can absorb oxygen to increase the number of Fe–O bonds at the CFS/MgO interface. In the thicker CFS layer, PMA disappeared, further indicating that the PMA originated at the interface. We attempted to quantitatively estimate the magnetic anisotropy energy (MAE) for these samples. However, because of the small signal-to-noise ratio, they did not give reasonable results.

3.3 Substrate temperature T_S dependence for the RF-sputtered sample

The dependence of T_S on the magnetic anisotropy is characterized in this section. The T_S was varied from RT to 350°C. The M–H curves for the CFS/MgO bilayers with various T_S are summarized in Fig. 2. Robust PMA was obtained over a wide T_S range between RT and 300°C. By contrast, the PMA disappeared in the sample formed at T_S = 350°C; the M_S was almost constant over the investigated T_S range.

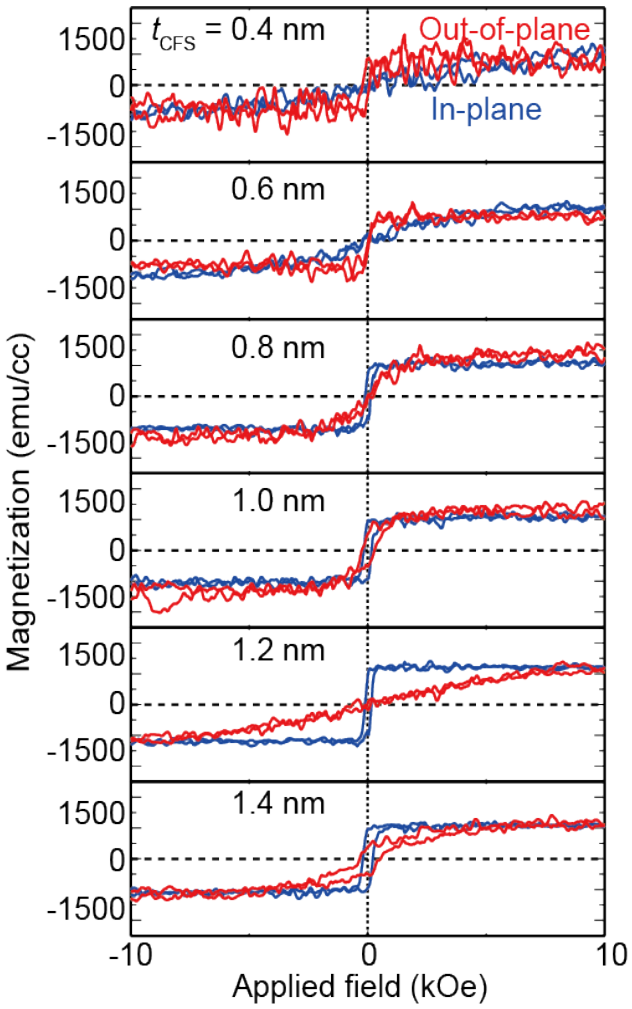

Fig. 4 Magnetization vs field curves for CFS/MgO bilayers formed at T_S = 350°C. The thickness of the CFS layers were varied from 0.4 nm to 1.4 nm.

Higher-temperature processes enable the formation of CFS layers with greater crystallinity; such layers are expected to exhibit greater spin polarization. To understand the change in the sample formed at T_S = 350°C, we further varied the thickness of the CFS layers for T_S = 300°C and 350 °C.

Figures 3 and 4 show M–H loops for CFS/MgO bilayers formed at T_S = 300°C and 350°C with various CFS thickness. For the T_S = 300°C samples, M–H loops with a high squareness ratio were observed between t_{CFS} = 0.4 nm and 0.7 nm. For the samples with $t_{CFS} \geq$ 0.8 nm, the easy axis was the in-plane direction. This change dramatically occurred when t_{CFS} was increased from 0.7 nm to 0.8 nm. We evaluated several samples and observed that this behavior was reproducible. The samples formed at T_S = 350°C exhibited PMA when t_{CFS} was less than 0.6 nm. Furthermore, thicker films exhibited in-plane anisotropy. Although the thickness range over which the CFS/MgO bilayers exhibited PMA was approximately the same, magnetic hysteresis loops for the samples prepared at T_S = 350°C changed gradually, whereas those for samples prepared at T_S = 300°C changed sharply.

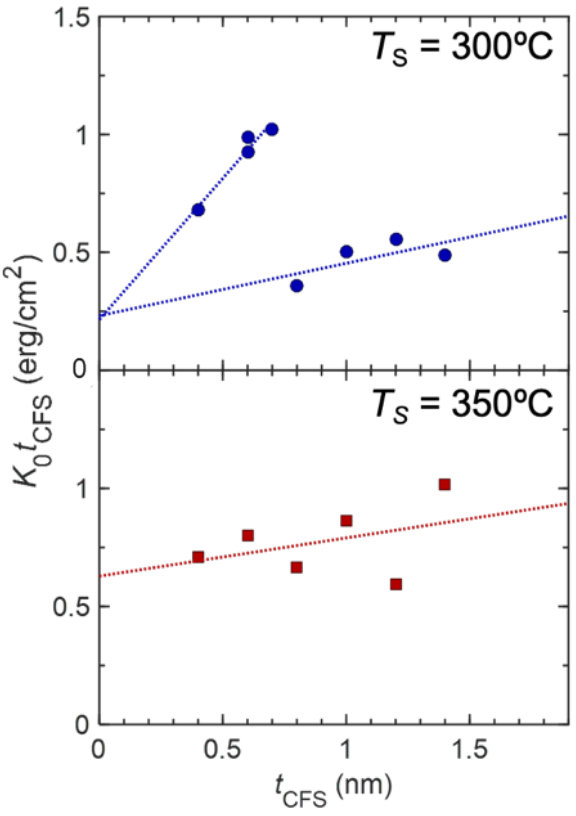

Fig. 5 K_0 t_{CFS} as a function of t_{CFS}.

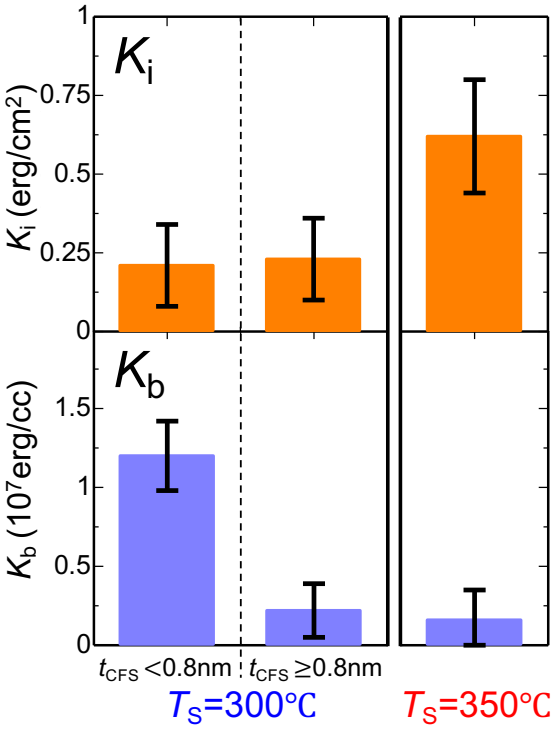

Fig. 6 Interfacial magnetic anisotropy K_i and film-originated magnetic anisotropy K_b extracted from the fitting.

3.4 Quantitative evaluation for T_S = 300°C and 350°C samples

We quantitatively analyzed the MAE in the samples from the *M*–*H* curves corresponding to the hard axis. The total of MAE, K_{tot}, is expressed as $K_0 - 2\pi M_S^2$, where K_0 is the uniaxial MAE in a bilayer and $2\pi M_S^2$ is the demagnetization energy in the CGS system of units. K_0 including interfacial PMA was further recorded as the following equation:[16]

$$K_0\, t_{CFS} = K_i + K_b t_{CFS} \quad \cdots (1)$$

where K_i is the interfacial MAE and K_b is the MAE of bulk CFS. Using this equation, we separately analyzed the contribution from the interface and that from the film itself.

Figure 5 shows the product of K_0 and t_{CFS} as a function of t_{CFS}. The top and bottom panels correspond to T_S = 300°C and 350°C, respectively. When T_S = 300°C, $K_0 t_{CFS}$ increased between 0.7 nm and 0.8 nm. In the other t_{CFS} range, $K_0 t_{CFS}$ proportionally increased with increasing t_{CFS}, as expressed in Eq. 1. For the sample formed at T_S = 350°C, $K_0 t_{CFS}$ well followed Eq. 1 and no jump was observed. Interestingly, the slope for the both series of samples was positive, indicating that the films in such an ultrathin range may exhibit uniaxial anisotropy in the out-of-plane direction.

The fitting results are summarized in Fig. 6. For the samples formed at T_S = 300°C, K_i did not change before and after the jump, whereas K_b increased more than fourfold by thinning t_{CFS}. However, the K_i of the samples formed at 350°C was much larger and the K_b was the same as that corresponding to T_S = 300°C with $t_{CFS} \geq 0.8$ nm.

The aforementioned results indicate that the structure of the CFS layers with $t_{CFS} < 0.7$ nm formed at T_A = 300°C might differ from that of the thicker CFS layers and might not have the $L2_1$ structure. This structural change, which might be caused by epitaxial stress, may lead to disruption of the half-metallicity. Demonstrating the half-metallicity in this ultrathin region would require further optimization of the buffer or capping layer.[25] In contrast, when the CFS layers were formed at T_S = 350°C, K_b did not change even in the ultrathin region; the K_b also matched that of the layers formed at T_S = 300°C. These results demonstrate that the structure near the interfaces is identical to that far from the interface, which was the $L2_1$ structure. Another important finding is that the contribution of the magnetic anisotropy in the film itself was out-of-plane. This new anisotropy might be induced by elastic stress[26] and warrants further investigation.

Summary

PMA in bilayers composed of ultrathin full-Heusler CFS alloy and MgO were systematically investigated. The CFS/MgO bilayers with RF-sputtered and reactively sputtered MgO layers were compared. Both techniques led to CFS/MgO bilayers with PMA, but oxygen exposure of the CFS surface was required to form the CFS/MgO

interface.

In addition, we characterized the PMA while varying the T_S for CFS sputtering. Robust PMA was observed at temperatures as high as T_S = 300°C. PMA in the sample formed at T_S = 350°C behaved differently when the thickness of the CFS layers was varied. Quantitative analysis of MAE density revealed that the interface and bulk contribution were dominant in the bilayers formed at 300°C and 350°C, respectively. Our findings should be useful in the further development of half-metallic ferromagnetic electrodes with PMA for next-generation spintronics devices.

Acknowledgements This work was supported by JSPS KAKENHI Grant Number 25889021, Kato Foundation for Promotion of Science, and Kenjiro Takayanagi Foundation. ICP-OES measurements were performed by the Ookayama materials analysis division, Technical Department, Tokyo Institute of Technology. The authors would like to thank MARUZEN-YUSHODO Co., Ltd. (http://kw.maruzen.co.jp/kousei-honyaku/) for the English language editing.

References

1) R.A. de Groot, F.M Muller, P.G. Van Engen, K.H.J. Buschow: *Phys. Rev. Lett.*, **50**, 2024 (1983).
2) J.H. Park, E. Vescovo, H.J. Kim, C. Kwon, R. Ramesh, T. Venkatesan: *Nature*, **392**, 794 (1998).
3) H. Ohmori, T. Hatori, S. Nakagawa: *J. Appl. Phys.*, **103**, 07A911 (2008).
4) D. Shum, et al.: *2017 Symposium on VLSI Technology*, Kyoto, Japan, T208 (2017).
5) S.S.P. Parkin, M. Hayashi, L. Thomas: *Science* **32**, 190 (2008).
6) L. Thomas, et al.: *J. Appl. Phys.*, **115**, 172615 (2014).
7) A.D. Kent, *Nature Mater.*, **9**, 699 (2010).
8) Y. Takamura, R. Nakane, S. Sugahara: *J. Appl. Phys.*, **105**, 07B109 (2009).
9) Y. Takamura, T. Suzuki, Y. Fujino, S. Nakagawa: *J. Appl. Phys.*, **115**, 17C732 (2014).
10) K. Shinohara, T. Suzuki, Y. Takamura, S. Nakagawa: *AIP Advances*, **8**, 055923 (2018).
11) N. Matsushita, Y. Takamura, Y. Fujino, Y. Sonobe, S. Nakagawa: *Appl. Phys. Lett.*, **106**, 062403 (2016).
12) H. Liu, Y. Honda, T. Taira, K. Matsuda, M. Arita, T. Uemura, M. Yamamoto: *Appl. Phys. Lett.,* **101**, 132418 (2012).
13) Y. Sakuraba, M. Ueda, Y. Miura, K. Sato, S. Bosu, K. Saito, M. Shirai, T. Konno, K. Takanashi: *Appl. Phys. Lett.*, **101** 2442-R (2012).
14) R. Shan, H. Sukegawa, W.H. Wang, M. Kodzuka, T. Furubayashi, T. Ohkubo, S. Mitani, K. Inomata, K. Hono: *Phys. Rev. Lett.*, **102**, 246601 (2009).
15) S. Maat, K. Takano, S.S.P. Parkin, E.E. Fullerton: *Phys. Rev. Lett.,* **87**, 087202 (2001).
16) S. Ikeda, K. Miura, H. Yamamoto, K. Mizunuma, H.D. Gan, M. Endo, S. Kanai, J. Hayakawa, F. Matsukura, H. Ohno: *Nature Mater.*, **9**, 721 (2009).
17) S. Yuasa, T. Nagahama, A. Fukushima, Y. Suzuki, K. Ando: *Nature Mater.*, **3**, 868 (2004).
18) T.L. Brown-Heft, J.A. Logan, A.P. McFadden, C. Guillemard, P.L. Fèvre, F. Bertaran, S. Andrieu, C.J. Palmstrøm: *Phys. Rev. Mater.*, **2**, 034402 (2018).
19) J. Okabayashi, J.W. Koo, H. Sukegawa, S. Mitani, Y. Takagi, T. Yokoyama: *Appl. Phys. Lett.*, **105** 122408 (2014).
20) Z. Wen, H. Sukegawa, S. Mitani, K. Inomata: *Appl. Phys. Lett.*, **98**, 242507 (2011).
21) P. Bruski, S.C. Erwin, M. Ramsteiner, O. Brandt, K.-J. Friedland, R. Farshchi, J. Herfort, H. Riechert: *Phys. Rev. B*, **83**, 140409(R) (2011).
22) T. Kubota, T. Kameda, J. Kim, A. Tsukamoto, S. Takahashi, Y. Sonobe, K. Takanashi: *Mater. Trans.*, **57**, 773 (2016).
23) Y. Jin, S. Valloppilly, P. Kharel, R. Pathak, A. Kashyap, R. Skomski, D.J. Sellmyer: *J. Phys. D,* **52**, 035001 (2019).
24) S. Wurmehl, G.H. Fecher, H.C. Kandpal, V. Ksenofontov, C. Felser, H.-J. Lin, J. Morais: *Phys. Rev. B*, **72**, 184434 (2005).
25) Y. Iida, J. Okabayashi, S. Mitani: *Appl. Phys. Lett.*, **113**, 252401 (2018).
26) S.C. Wu, G.H. Fecher, S.S. Naghavi, C. Felser: *J. Appl. Phys.*, **125**, 082523 (2019).

Received Feb. 18, 2019; Revised July. 29, 2019; Accepted Sep. 11, 2019

ファイル名 ： 2019MSJ_takamura_著者最終稿.docx

フォルダー ：

/Users/yotatakamura/Library/Containers/com.microsoft.Word/Data/Documents

テンプレート ： /Users/yotatakamura/Library/Group Containers/UBF8T346G9.Office/User Content.localized/Templates.localized/Normal.dotm

表題 ： Camera-Ready Format for JMSJ

副題 ： 2004 April

作成者 ： Shigeki

キーワード ：

説明 ：

作成日時 ： 2020/02/05 15:43:00

変更回数 ： 2

最終保存日時 ： 2020/02/05 15:43:00

最終保存者 ： Yota Takamura

編集時間 ： 1 分

最終印刷日時 ： 2020/02/05 15:43:00

最終印刷時のカウント

ページ数 ： 5

単語数 ： 2,762 (約)

文字数 ： 15,748 (約)